A Technique for Extrapolating Numerically Rigorous Solutions of Electromagnetic Scattering Problems to Higher Frequencies and Their Scaling Properties

Zwi Altman, *Senior Member, IEEE,* and Raj Mittra, *Life Fellow, IEEE*

***Abstract*— The possibility of extrapolating the current distribution on two-dimensional scatterers to high frequencies, from the knowledge of the solution at two or more lower frequencies, is investigated in this paper. A simple extrapolation algorithm is developed in which the current distribution is first calculated at two lower frequencies, and then split into propagating or decaying traveling wave components in the lit and shadow regions. These components are scaled to higher frequencies, by using simple operations such as stretching of the magnitude and linear extrapolation of the phase. This technique enables one to solve a class of large-body scattering problems, well beyond the range of rigorous numerical techniques. Furthermore, the extrapolated solution is rapidly constructed over a very wide range of frequencies, typically by utilizing the rigorous solution at only two lower frequencies. The application of the extrapolation algorithm is demonstrated for several examples, viz., an ellipse with a high aspect ratio, and wing-shaped geometries with rounded and sharp edges. The robustness of the technique is illustrated by considering grazing angles of incidence where the asymptotic techniques typically break down.**

***Index Terms*—Electromagnetic scattering by rough surfaces.**

I. Introduction

NUMERICALLY rigorous approaches to frequency domain electromagnetic scattering problems, e.g., the method of moments (MoM) or the finite-element method (FEM), can become extremely expensive in terms of memory requirement and central processing unit (CPU) time when dealing with a large scatterer, especially when the solution is needed over a broad band of frequencies. One approach to obviating this problem is to solve as large as a problem as can possibly be accommodated on the available computer, and then attempt to extrapolate the solution to higher frequencies. Despite the great need for solving large body problems using numerical rather than asymptotic techniques, the extrapolation technique [1] has not received as much attention in the literature as it probably deserves. In [1] an extrapolation technique has been combined with the MoM to solve scattering problems from large bodies of revolution, and the possibility of extrapolating entire domain basis functions of complex exponential type has been studied.

Manuscript received December 18, 1995; revised September 30, 1996.

Z. Altman is with CNET, National Center of Telecommunication Studies of France Telecom, 92794 Issy les Moulineaux, France.

R. Mittra is with the Electromagnetic Communication Research Laboratory, Pennsylvania State University, University Park, PA 16802 USA.

Publisher Item Identifier S 0018-926X(99)04783-3.

In this paper, we examine the extrapolation problem by posing the following question: Assuming that the MoM solution for the current distribution has been generated for a few (two or more) frequencies for which the body is at least moderately large in terms of wavelength and yet is manageable in size, is it possible to accurately predict the solution for higher frequencies for which the body is too large to be handled using the available resources?

We show in this paper that the answer is indeed in the affirmative for the cases of the geometries investigated, even for the situation where the conventional asymptotic methods typically fail, e.g., for grazing incidence. The extrapolation technique is based on a frequency scaling procedure in which the computed current distribution on the body is first split into general constituent traveling components, each of which is then extrapolated, individually, by using algorithms described in this paper. We use the term *scaling* for extrapolation of a single traveling wave constituent in contrast to *extrapolation* which is employed for the total current distribution that can include one or several traveling waves. The individual scaling is necessitated by the fact that the different components of the current distribution follow different scaling laws. This is explained on detail in Section II.

To illustrate the versatility of the extrapolation approach, we examine three different types of scatterers in this paper. The first of these is an ellipse with a high aspect ratio which is a typical example of a geometry of a smooth scatterer, and which supports only a single traveling wave at each point of the surface when the scatterer size is large. Next, we turn to a wing-shaped geometry with a sharp edge, which launches edge-diffraction currents that scale differently [2] than does the physical optics component. Finally, the third case studied is a modification of the previous wing-shaped geometry whose edges are now rounded. This case is of particular interest since the surface has a slope discontinuity that causes an additional traveling wave to be excited for the TE polarization. The scaling properties of the constituent components in the lit, shadow and the transition regions are discussed in detail in Section V.

II. Scaling of the Physical Optics Current Distribution

Consider three perfect conducting surfaces S_1, S_2 and S_3, as shown in Fig. 1, which may be viewed as the surface of a

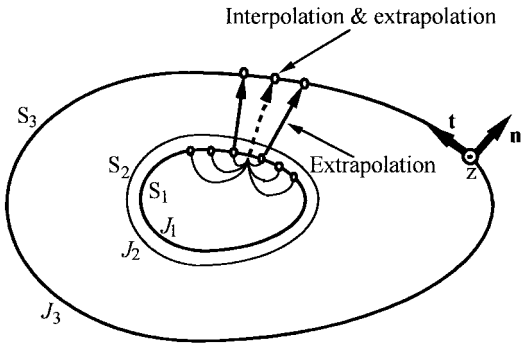

Fig. 1. Three surfaces in a wavelength scale that represent a scatterer at three different frequencies.

given scatterer at three different frequencies in a wavelength scale. The surfaces S_2 and S_3 are related to S_1 via a stretching procedure, because their geometries satisfy the following relationship:

$$\forall \mathbf{r} \in S_1 \rightarrow \begin{cases} p\mathbf{r} \in S_2 \\ t\mathbf{r} \in S_3 \end{cases} \tag{1}$$

where p and t are constant positive numbers. If $f_1(\mathbf{r})$ is a scalar function on S_1 we define the stretched function $f_1^s(t\mathbf{r})$ on S_3 as

$$f_1^s(t\mathbf{r}) \equiv f_1(\mathbf{r}). \tag{2}$$

Assume that S_1 is illuminated by a plane wave $\mathbf{H}^i = \mathbf{H}_0 e^{-j\mathbf{k}\cdot\mathbf{r}}$, where $\mathbf{k}$ is the vector wave number. In the lit region, the physical optics (PO) approximation to the current distribution $\mathbf{J}$, which is often employed for large smooth scatterers, is given by

$$\mathbf{J}_{\rm po} = 2\hat{\mathbf{n}} \times \mathbf{H}^i. \tag{3}$$

Let $\phi_1 = \mathbf{k}\cdot\mathbf{r}$ and $\phi_2 = \mathbf{k}\cdot p\mathbf{r}$ be the phases of the current distributions $\mathbf{J}_{1\rm po}$ and $\mathbf{J}_{2\rm po}$ on S_1 and S_2, respectively. Then the PO approximation to $\mathbf{J}_3$ can be written as

$$\mathbf{J}_{3\rm po} = (\hat{\mathbf{n}} \times \hat{\mathbf{h}}_0) J_{1\rm po}^s(t\mathbf{r}) e^{-j(\mathbf{k}\cdot\mathbf{r} + \Delta_\phi \frac{t-1}{p-1})}; \quad \Delta_\phi = \phi_2 - \phi_1 \tag{4}$$

where $\hat{\mathbf{h}}_0$ is a unit vector parallel to $\mathbf{H}_0$. Equation (4) states that in order to calculate $\mathbf{J}_{3\rm po}$ from $\mathbf{J}_{1\rm po}$ and $\mathbf{J}_{2\rm po}$, we need to stretch the magnitude of $\mathbf{J}_{1\rm po}$ to the new surface and perform a linear extrapolation for the phase. Equation (4) is obviously an example of scaling, since the value of the function at a stretched point $t\mathbf{r}$ depends on the value of the function at points $p_i\mathbf{r}$ on other surfaces. However, the above scaling procedure, though simple, is not sufficiently general to be applicable to other components of the current, as we will soon see. An important objective of this work is to extend the extrapolation procedure to a more general current distribution of the type encountered in the geometries investigated in this paper.

III. Scaling of One Traveling Wave Current Component

The first step to developing a general scaling procedure is to realize that different components of the surface current distribution must be scaled differently, i.e., a single scaling algorithm is not universally applicable to the total current distribution. For the sake of simplicity of notation, let us assume that the current J_i represents one of the components of the total current distribution, viz., J_z (axial) for the TM case and J_t (transverse) for the TE case. Let J_1, J_2, and J_3 be the current distributions on the surfaces S_1, S_2, and S_3, respectively. Also let J_1 and J_2 be obtained by employing a numerically rigorous technique, e.g., the MoM or FEM. Our objective is to derive J_3 from J_1 and J_2 via a scaling procedure.

As a first approximation to J_3, we stretch the magnitude of J_1 by computing $J_1^s(t\mathbf{r})$, and extrapolating the phase linearly, as in (4), to get

$$\begin{cases} \phi_1 = \text{phase}[J_1(\mathbf{r})] \\ \phi_2 = \text{phase}[J_2(\mathbf{r})] \\ J_3 = \left|J_1^s(t\mathbf{r})\right| e^{-j(\phi_1 + \Delta_\phi \frac{t-1}{p-1})}; \quad \Delta_\phi = \phi_2 - \phi_1. \end{cases} \tag{5}$$

The phase scaling is linear so long as the surface currents on S_1 consist of a single traveling wave. The choice of linear scaling of the phase can be intuitively explained as follows: Let us denote the length parameter along the surface by s, and the propagation constants of the traveling waves at s and ts on S_1 and S_3, respectively, by $\beta_1(s)$, and $\beta_3(ts)$. Then, the phase accumulation $d\phi_1(s)$ due to propagation along dl is given by $\beta_1(l)\,dl$, and integrating $d\phi_1$ along the path of propagation yields the desired result for the phase. The above result is based on the Ansatz that $\beta_3(ts) \approx \beta_1(s)$, which we will verify later numerically. The phase at ts on S_3 is thus approximated as

$$\phi_3(ts) = \int_{s_o}^{s} \beta_3(tl) d(tl) \approx t\phi_1(s). \tag{6}$$

Obviously, when the current on the scatterer constitutes more than one traveling wave, the individual contributions must be scaled separately, since their wave numbers are different.

As the surface S_3 expands, i.e., the scaling parameter t is increased, the current distribution evolves, and it often approaches the PO limit. We take advantage of this knowledge by modifying (5) that incorporates this limit for large S_3. Toward this end we define $\Delta_r(\mathbf{r})$ and the deviation function $D(\mathbf{r})$ from the PO limit as follows:

$$\Delta_r(\mathbf{r}) \equiv (t-1)r \tag{7a}$$

$$D(\mathbf{r}) \equiv |J_{3\rm po}(t\mathbf{r})| - \left|J_1^s(t\mathbf{r})\right|. \tag{7b}$$

Finally, we represent the magnitude of the scaled solution for the current via the equation

$$|J_3| \cong \left|J_1^s\right| + \left(1 - e^{v(\mathbf{r})\Delta_r(\mathbf{r})}\right) D(\mathbf{r}) \tag{8}$$

where $v(\mathbf{r})$ is determined for each $\mathbf{r}$ by substituting $|J_2|$ into the left hand side of (8) and solving for $v(\mathbf{r})$. Equations (5) and (8) will be verified numerically for the four cases that are discussed in the following two sections.

IV. TM Case

Consider a two-dimensional metallic scatterer with an elliptical geometry with a 5:1 aspect ratio. The geometrical parameters for the three surfaces, S_1, S_2 and S_3 (Fig. 1) are

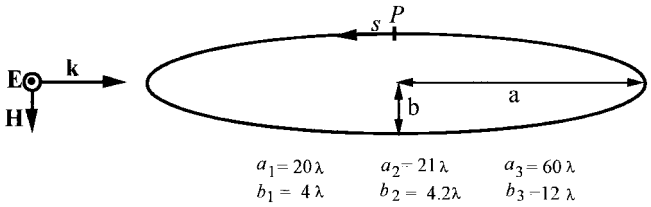

Fig. 2. A PEC scatterer with an elliptical geometry illuminated by a TM incident plane wave at grazing incidence. The parameters a_i and b_i correspond to the surfaces S_i of Fig. 1.

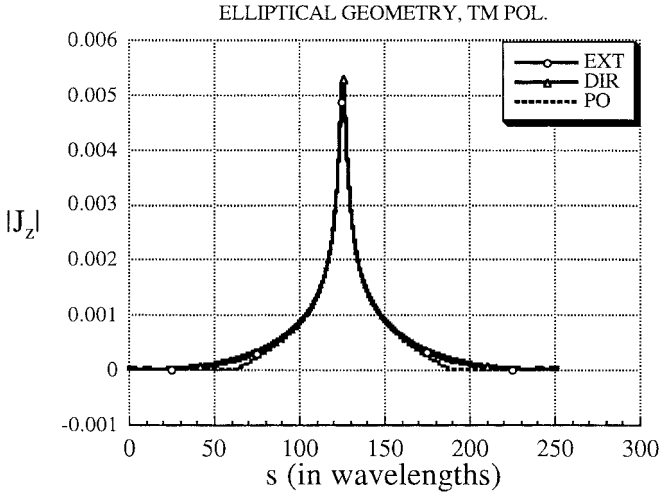

Fig. 3. Current distributions on the elliptical scatterer as a function of the distances measured from the transition point P (Fig. 2). The extrapolated solution is compared to the direct MoM and the physical optics solutions.

given in Fig. 2, and the scaling factor is $t = 3$ in this example. Let a TM-polarized plane wave be incident on the scatterer at grazing. The results for the magnitude of the induced current distribution for the scaled solution (EXT), the direct MoM solution (DIR) and the PO approximation are shown in Fig. 3. The MoM solutions throughout this work have been calculated by using a combined field integral equation (CFIE) formulation to avoid the internal resonance problem. The accuracy of the scaling procedure is demonstrated by the excellent agreement between the scaled and direct solutions throughout, while the PO and direct solutions are seen to differ from each other in the transition region. It is evident that the transition of the surface current from the lit to the shadow region must be smooth; however, the PO approximation predicts that the current goes to zero abruptly in the shadow region because the normal to the surface is parallel to the H-field at the shadow boundary. In contrast to the TE case, there is no discontinuity in the current distribution for the TM polarization and, therefore, the PO approximation is good for smooth geometries for the latter case. The far-field results are shown in Figs. 4 and 5. The scaled result is almost identical to the direct solution whereas the PO approximation has a spurious null close to the forward scattering angle. In the backscattering region the PO solution is off by approximately 1 dB.

Next, let us consider the scattering problem by a body with an edge. Referring to the canonical solution of the edge diffraction problem [2], we can easily verify that at the edge the solution tends to its electrostatic limit and, therefore, does

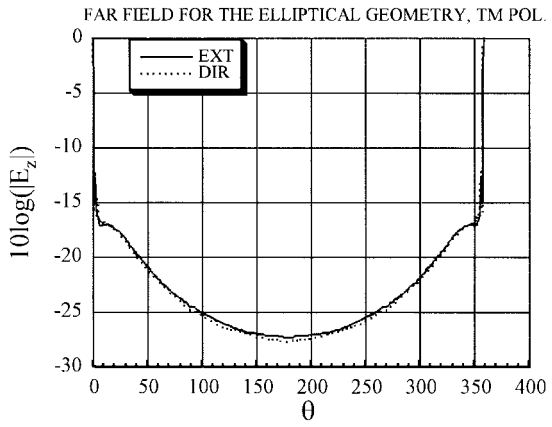

Fig. 4. Far-field results for the elliptical geometry with TM excitation. Comparison between the extrapolated and direct solutions.

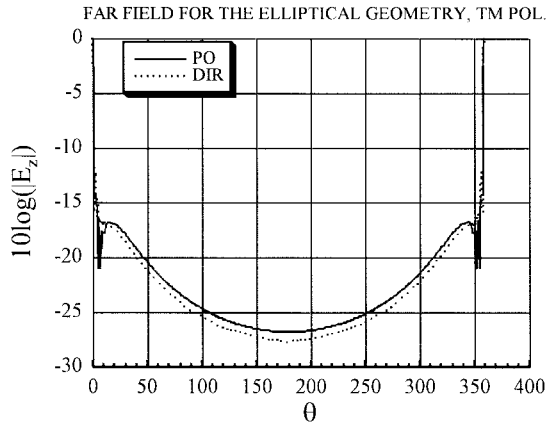

Fig. 5. Far-field results for the elliptical geometry with TM excitation. Comparison between the direct and PO solutions.

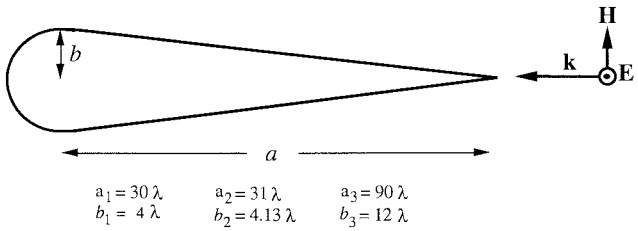

Fig. 6. A wing-shaped geometry with a sharp edge illuminated by a TM incident plane wave. The front part consist of a portion of a circle of radius b, and a is the distance between the center of the circle and the edge. The parameters a_i and b_i correspond to the surfaces S_i of Fig. 1.

not scale. However, sufficiently far from the edge, the solution tends asymptotically to the PO limit. We may therefore modify the scaling procedure for scatterers with edges as follows. In the region far from the edge, where the magnitude of the current distribution settles down to the PO limit, we use (5), whereas close to the edge we choose $|J_3(s)| = |J_1(s)|$, i.e., we leave the magnitude unstreched. The phase distribution, however, is extrapolated linearly according to (5).

Let us now verify the accuracy of this approximation for a wing-shaped scatterer, which is illuminated by a TM plane wave as shown in Fig. 6, for a scaling factor of $t = 3$. The magnitude of J_3 at a distance of $d = 20\lambda$ from both sides

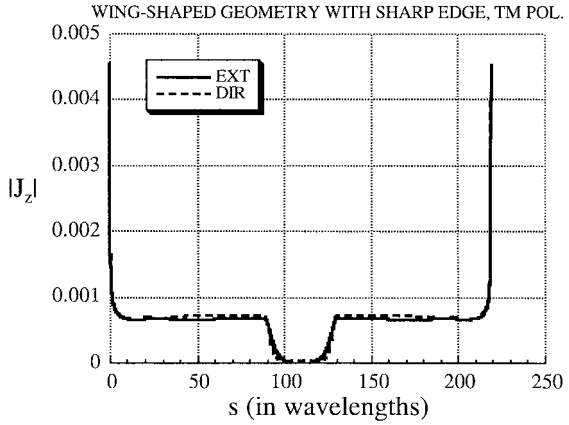

Fig. 7. Current distributions for the wing-shaped geometry with a sharp edge. Comparison between the extrapolated and direct MoM solutions.

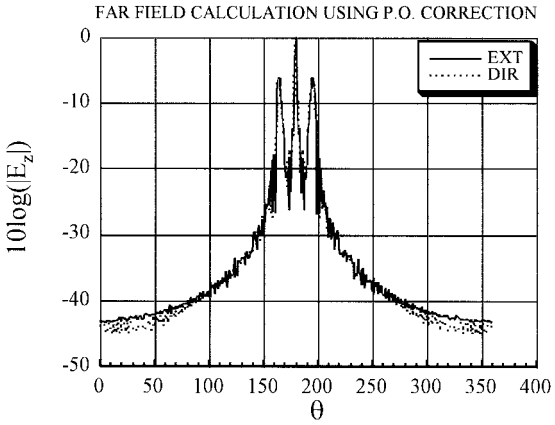

Fig. 9. Comparison between the extrapolated and direct solutions. A phase correction is obtained using PO approximation for the current.

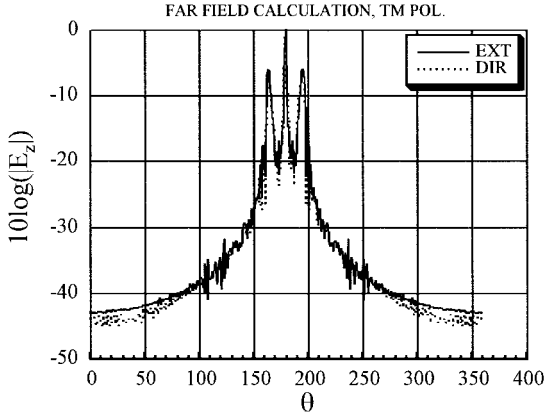

Fig. 8. Far-field results for the wing-shaped geometry with sharp edge and TM excitation. Comparison between the extrapolated and direct solutions.

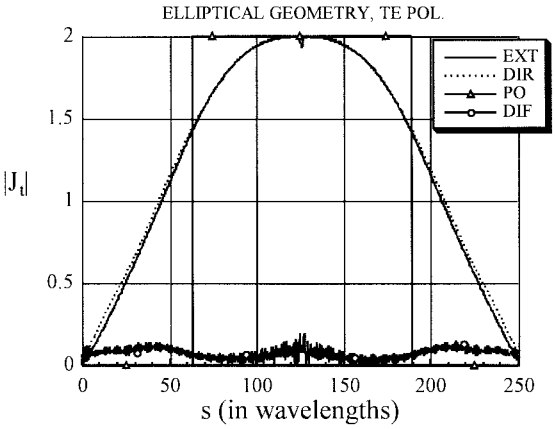

Fig. 10. Current distributions for the elliptical scatterer of Fig. 2 with TE excitation. The parameters for the three surfaces S_1, S_2, and S_3 are $a_1 = 20$, $b_1 = 4$, $a_2 = 25$, $b_2 = 5$, $a_3 = 60$, and $b_3 = 12$. The extrapolated solution is compared to the direct MoM and the PO solutions. The difference between the direct solution and the extrapolated one is shown by the bottom curve.

of the edge is not stretched, whereas the phase is linearly extrapolated everywhere. The choice for d (20λ in our case) is flexible, however it should be taken big enough for the solution to settle down to the PO limit to avoid discontinuities in the current distribution. It should be noted that by processing more than two solutions (J_1 and J_2 in our case) one could find closed form expressions for the current distribution as a function of size or frequency in the presence of edges [3]. The scaled and direct solutions for the current distribution are shown in Fig. 7. The two curves, which are almost identical to each other, validate the proposed scaling procedure for the magnitude of the current density in the vicinity of the edge. Although small differences of the extrapolated and MoM currents phase were found to be present in the lit region, they had little influence on the far-field pattern. In Fig. 8, we compare the extrapolated and direct far-scattered fields. The two curves are seen to agree well for most angles, except in the region around 120° and 240°, where some oscillations appear in the extrapolated solution. However, as shown in Fig. 9, the undesired oscillations disappear if we replace the phase of the extrapolated solution by that of the PO solution at distances of 20λ and beyond from the edges. Thus, we have shown that a highly accurate solution can be obtained for this geometry by combining the scaled solution with the PO approximation. Not unexpectedly, the PO only far-field pattern was found to exhibit large errors since the fringe currents have a significant contribution to the far-field of this scatterer.

V. TE Case

In this section we consider the case of TE polarization for which the results have some interesting differences from the TM case. In the lit region, the incident magnetic field in the TE case is perpendicular to the normal to the surface; consequently, the amplitude of the current distribution at the transition region is much higher for the TE than it is for the TM case. The PO approximation is rather poor in the transition region because it drops abruptly as we transition from the lit region to the shadow region. This nonphysical discontinuity in the PO approximation of the current distribution generates large spurious oscillations in the far-field pattern.

When the surface of the scatterer and its slope are continuous, we expect only one traveling wave to be excited along the surface at each point. Equations (5) and (8) can then be used to extrapolate the current components to higher frequencies. As an example, consider again the case of the ellipse shown in Fig. 2 for the case of TE illumination and a scaling factor of $t = 3$. The current distribution for the extrapolated, direct and

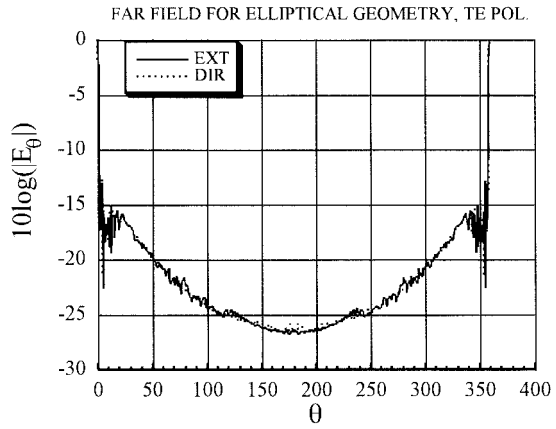

Fig. 11. Far-field results for the elliptical geometry with TE excitation. Comparison between the extrapolated and direct solutions.

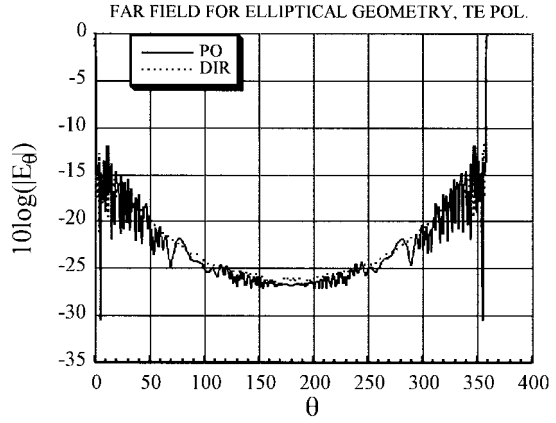

Fig. 12. Far-field results for the elliptical geometry with TE excitation. Comparison between the direct and PO solutions.

PO solutions are plotted in Fig. 10. The difference between the extrapolated and the direct solution is also shown by the bottom curve in the same figure, and this curve serves as an indicator of the quality of the extrapolated result for both the magnitude and phase. Because the aspect ratio of the ellipse is large, the "PO region" with constant magnitude is very small, whereas the transition region is very large; thus, the PO approximation is relatively poor in this case. The comparisons between the various far-field patterns are presented in Figs. 11 and 12. An excellent agreement between the extrapolated and direct solutions is observed in Fig. 11, whereas the PO pattern, shown in Fig. 12, is seen to have nonphysical oscillations due to the discontinuous behavior of the current in the transition region.

Let us now return to an important case where the slope of the surface is not continuous. All of our numerical experiments show that, unlike the TM case, a TE illumination at a slope discontinuity excites more than one traveling wave. This implies that direct extrapolation of the current distribution is not possible since each traveling wave must be scaled differently.

As an example, let us consider the scatterer of Fig. 13, with a scaling factor of $t = 2$. Analyzing the current distribution we find that two traveling waves are excited at each of the

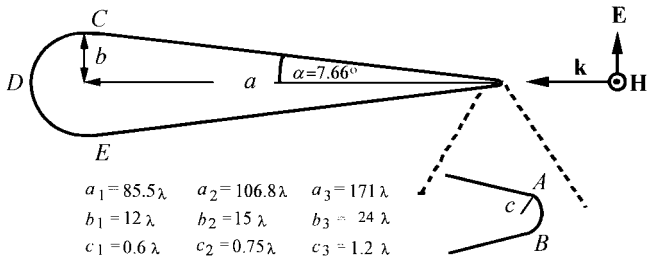

Fig. 13. A wing-shaped geometry with a rounded edge illuminated by a TE incident plane wave. The front and back regions consist of portions of circles with radii b and c, respectively, and a is the distance between the centers of the two circles. The length parameter s along the curve is measured from B and increases in the counterclockwise direction.

slope discontinuities A and B, and they both travel in the same direction. In the lit region, and away from the slope discontinuities, the propagation constants associated with these two traveling waves are found to be very close to each other, these constants being $\beta_{\rm I} = 6.227$ ($=2 * \pi * \cos\alpha$, which corresponds to the PO approximation), and $\beta_{\rm II} = 6.282$. The two traveling waves propagate in the same direction, and thus introduce an interference pattern with a very slow beat frequency along the straight section of the scatterer. In Fig. 14, we compare the stretched solution $J_1^s(ts)$ on S_3 [see (2)] and J_3.

When we increase the angle α (see Fig. 13), we find that the magnitude of the oscillations decreases while their frequency increases, and the solution approaches the PO limit. For $\alpha = 30°$, for example, the magnitude of the oscillations is less than a third of that at 7.66°, and its period is smaller. For $\alpha = 60°$, the oscillations become essentially negligible.

It is obvious that we cannot obtain J_3 from J_1 by a simple scaling of the total current distribution using (5) and (8), since the forms of the curves are completely different. We show, however, that a simple extrapolation procedure based on selective scaling of the two traveling waves-components is still possible. Let us denote these components by the subscripts "po" and "tw." We calculate $J_{\rm po}$ by using (3), and then obtain $J_{\rm tw}$ by calculating the difference between the total current distribution and $J_{\rm po}$. Next, we write the total current distributions on S_1 and S_2 in the form

$$J_1 = J_{1\rm po} + J_{1\rm tw} \tag{9a}$$

$$J_2 = J_{2\rm po} + J_{2\rm tw}. \tag{9b}$$

Finally, we calculate $J_{3\rm tw}$ by scaling $J_{1\rm tw}$ using (5), and then adding $J_{3\rm po}$ to it using (3), to obtain the total current distribution.

Let us now turn to the shadow region. Since the two traveling waves penetrate the shadow region at C, they should be scaled separately in this region also. However, since the extension of the PO traveling wave in the shadow region is not known analytically, we can no longer separate the two contributions as we did in the lit region [see (9)], and we deal with this case as follows. We assume that the shadow region is sufficiently large and, hence, the traveling waves are negligible

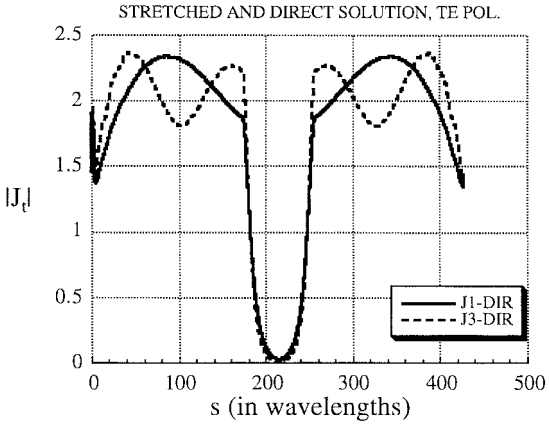

Fig. 14. Comparison between the stretched current at a low frequency to the direct solution at a higher frequency.

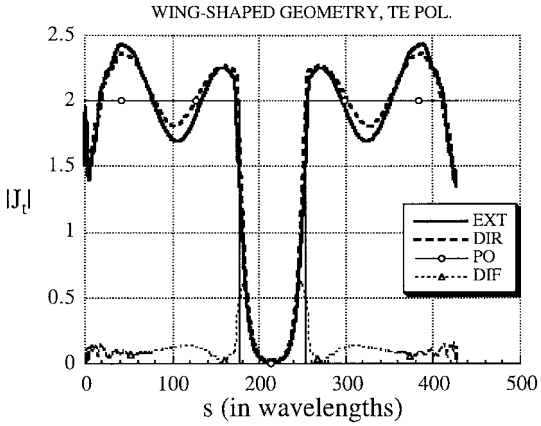

Fig. 15. Current distributions for the wing-shaped geometry with a rounded edge. The extrapolated solution is compared to the direct MoM and the PO solutions. The difference between the direct solution and the extrapolated one is given by the bottom curve.

at D (Fig. 13). We then compute $|J_3|$ from (8), and denote the normalized to one function $|J_3|/|\max(|J_3|)|$ at the shadow region by $p(s)$, the "profile" function. The next step is to derive the two propagating constants $\beta_{3\mathrm{po}}$ and $\beta_{3\mathrm{tw}}$. The first one is derived straightforwardly from the analytical representation of the PO current. We extract the second propagating constant, viz., $\beta_{3\mathrm{tw}}$, via the GPOF algorithm [4], [5], by sampling the current at a few points in the lit region just before the transition point C^-. Since $\beta_{3\mathrm{po}}$ and $\beta_{3\mathrm{tw}}$ are quite close to each other, we assume that they have the same profile function $p(s)$. We then denote the complex amplitudes of the scaled components $J_{3\mathrm{tw}}$ and $J_{3\mathrm{po}}$, respectively, at C^-, by $A_{3\mathrm{tw}}$ and $A_{3\mathrm{po}}$. Finally, we postulate the following representation for the current distribution in the shadow region between C and D

$$J_3(s) \approx A_{3\mathrm{po}} p(s) e^{j\beta_{3\mathrm{po}} s} + A_{3\mathrm{tw}} p(s) e^{j\beta_{3\mathrm{tw}} s}. \qquad (10)$$

Note that in the above representation, the decay of the current in the shadow region has been accounted for by the profile function $p(s)$; hence, there is no need to include an attenuation constant in the exponents.

Although the representation in (10) is quite accurate for our purposes, it may be further improved, if desired, as follows. Examining the propagation constants at different points along the surface, we find that their values increase slightly as the wave penetrates into the shadow region. Thus, to obtain an even more accurate representation of J_3, we can let $\beta_{3\mathrm{po}}$ and $\beta_{3\mathrm{tw}}$ in J_3 vary between C and D in the same manner as they do in J_1.

The results for the current distribution for the extrapolated, direct and PO solutions are plotted in Fig. 15. The difference between the extrapolated an direct solution is also shown by the bottom curve in the same figure. We can see that by selective scaling of the two traveling waves, we can extrapolate the current distribution accurately to higher frequencies even though the shapes of the curves $|J_1|$ and $|J_2|$ are completely different from that of $|J_3|$. From the current difference plot we can see a small error in phase in the shadow region which accumulates as the traveling waves go deeper into that region.

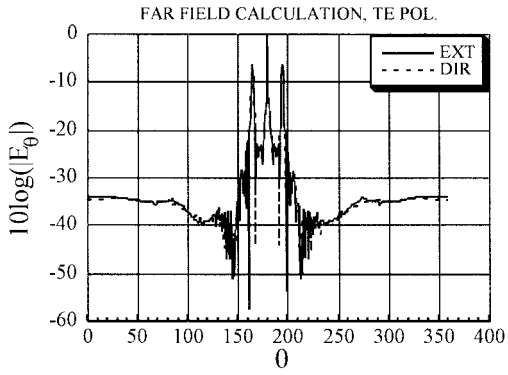

Fig. 16. Far-field results for the wing-shaped geometry with a rounded edge and TE excitation. Comparison between the extrapolated and direct solutions.

Since the transition in both phase and magnitude are very smooth, the small error in the phase does little to affect the far-field pattern, as is evident form Fig. 16, which shows that the far-field patterns of the extrapolated and direct solutions almost overlap. Finally, we compare the far-field patterns of the PO approximation and the direct solution in Fig. 17. The PO solution is seen to deviate noticeably from the direct solution over a wide angular range. This is because the PO approximation of the current does not include the second traveling wave in the lit region and has a nonphysical behavior in the transition region.

Next, we attempt to estimate the contribution of the second traveling wave in the current distribution on the far-field. We do this by constructing a hybrid solution that excludes this traveling wave component and consists, instead, of only the PO approximation in the lit region and its extension in the shadow region. This study is important because it sheds light into the accuracy behavior of numerical techniques that attempt to hybridize the high frequency scattering solution by using the PO approximation on the smooth portion of the scatterer and a rigorous technique, e.g. MoM or FEM, in the neighborhood of a discontinuity. We have already shown that the influence of the discontinuity is not localized, and that the slope disconti-

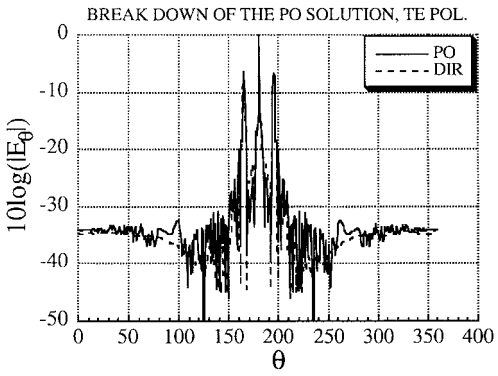

Fig. 17. Far-field results for the wing-shaped geometry with a rounded edge and TE excitation. Comparison between PO and direct solutions.

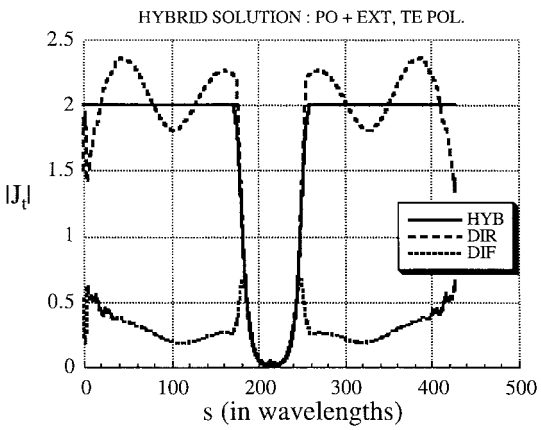

Fig. 18. Comparison of the hybrid solution for the current distribution with the direct solution. The difference curve represents the contribution of the second traveling wave.

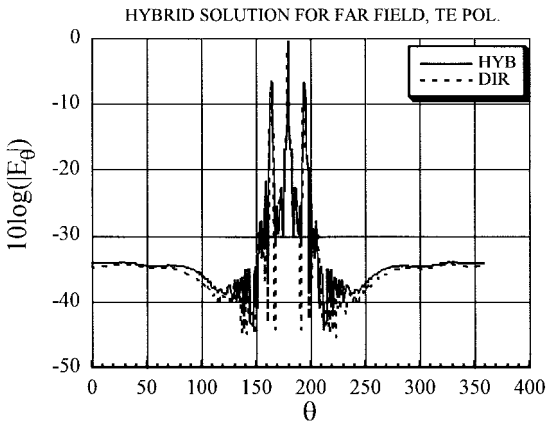

Fig. 19. Far-field results for the wing-shaped geometry with rounded edge and TE excitation. Comparison between the hybrid and direct solutions.

nuity can excite a traveling wave that propagates for hundreds of wavelengths with little decay. However, as we show below, this may not have a significant effect on the far-field.

In Fig. 18, we compare the hybrid and direct solutions and also plot the difference curve which shows the contribution of the second traveling wave. The level of the difference curve implies that the hybrid solution introduces a significant error in the near field. We next examine the far-field pattern for the hybrid and direct solutions plotted in Fig. 19. The two curves are seen to be very similar, with only some minor differences in their levels. This interesting result can be explained by observing that, away from the slope discontinuity, the propagation constants of the two traveling waves are very close to each other, viz., 6.227 and 6.282; hence their far-field patterns are virtually indistinguishable from each other. If we increase the angle of incidence, or the wedge angle α, the difference between the propagation constant increases. However, the amplitude of the second traveling wave decreases at the same time, so that its influence on the far-field pattern remains relatively small.

VI. Conclusion

In this work we have examined the two-dimensional scattering problem for a number of scatterers, and have presented an extrapolation procedure based on the selective scaling properties of constituent current components on the surface of the scatterer. We have shown how we can derive the extrapolated current at high frequencies from the knowledge of the numerical solution at two lower frequencies, where the body is only moderately large. Thus the method has the potential for application to very large body scattering problems, at least for a class of canonical scattering geometries that may be used as benchmarks for numerically rigorous solution techniques.

The extrapolation is based on selectively stretching the magnitude and linearly extrapolating the phase of the constituent current components. The extrapolation procedure has the attractive features that it is simple to implement and very efficient in terms of the CPU time. It is also more accurate than the PO, especially at grazing incidence where PO tends to break down. Furthermore, unlike asymptotic methods, it does not rely upon the availability of canonical solutions and it can handle both the transition and shadow regions with relative ease. It can be applied to scatterers with both slope discontinuities and edges.

It may also be possible to combine the extrapolation technique with the conventional MoM, by employing subdomain basis functions for the complex portions of the scatterer in a manner proposed by Wang, *et al.* [6]–[8], to handle more complex geometries than have been investigated in this paper.

The extension of the extrapolation procedure is currently being investigated for a class of three-dimensional scattering problems [3]. In order to get accurate results, one must first generate the solution at several lower frequencies from which the solution is extrapolated to higher frequencies. The solutions at lower frequencies can then be used to determine accurately the frequency dependency of the solution. The finite difference time domain technique is found to be very well suited for this problem since in one run one can get the solution over a wide band of frequencies.

Acknowledgment

The authors would like to thank to Prof. A. F. Peterson for his assistance and for the CFIE MoM code, and to the NCSA for generously providing CPU time on the SGI computers.

REFERENCES

[1] Z. Altman and R. Mittra, "Combining an extrapolation technique with the method of moments for solving large scattering problems involving bodies of revolution," *IEEE Trans. Antennas Propagat.*, vol. 44, pp. 548–553, Apr. 1996.

[2] R. Mittra and S. W. Lee, *Analytical Techniques In The Theory Of Guided Waves*. New York: Macmillan, 1971, ch. 1.

[3] J. C. Goswami and R. Mittra, "On the solution of a class of large-body scattering problems via the extrapolation of FDTD solutions, " *J. Electromagn. Waves Applicat.*, vol. JEWA 12, no. 2, pp. 229–244, 1998.

[4] Z. Altman, R. Mittra, O. Hashimoto, and E. Michielssen, "Efficient representation of induced currents on large scatterers using the generalized pencil of function method," *IEEE Trans. Antennas Propagat.*, vol. 44, pp. 51–57, Jan. 1996.

[5] Y. Hua and T. K. Sarkar, "Generalized pencil of function method for extracting poles of an EM system from its transient response," *IEEE Trans. Antennas Propagat.*, vol. 37, pp. 229–234, Feb. 1989.

[6] L. N. Medgyesi-Mitshang and D. S. Wang, "Hybrid solutions for large-impedance coated bodies of revolution," *IEEE Trans. Antennas Propagat.*, vol. 34, pp. 1319–1329, Nov. 1991.

[7] J. M. Bornholdt and L. N. Medgyesi-Mitschang, "Mixed-domain Galerkin expansions in scattering problems," *IEEE Trans. Antennas Propagat.*, vol. 36, pp. 216–227, Feb. 1988.

[8] D. S. Wang, "Current-based hybrid analysis for surface-wave effects on large scatterers," *IEEE Trans. Antennas Propagat.*, vol. 39, pp. 839–850, June 1991.

Zwi Altman (S'88–M'89–SM'99) received the B.Sc. and M.Sc. degrees in electrical engineering from the Technion-Israel Institute of Technology, Haifa, in 1986 and 1989, respectively, and the Ph.D. degree in electronics from the Institut National Polytechnique de Toulouse, France, in 1994.

He was a "Lauréat de la Bourse LAVOISIER" of the French Foreign Ministry in 1994, and from 1994 to 1996 he was a Postdoctoral Research Fellow in the Electromagnetic Communication Laboratory, Electrical Engineering Department, University of Illinois. In 1996 he joined the CNET—National Center of Telecommunication Studies of France Telecom. His research interests include computational electromagnetics, electromagnetic compatibility, bio-electromagnetics, wavelets, and genetic algorithms.

Dr. Altman is currently an Associate Editor for the IEEE TRANSACTIONS ON ELECTROMAGNETIC COMPATIBILITY.

Raj Mittra (S'54–M'57–SM'69–F'71–LF'96) received the M.S. degree from the University of Calcutta, India, and the Ph.D. degree from the University of Toronto, Canada.

He is with the Electromagnetic Communication Research Laboratory, Pennsylvania State University, University Park.

Dr. Mittra is Past President of the Antennas and Propagation Society and Past Editor of the IEEE TRANSACTIONS ON ANTENNAS AND PROPAGATION. He received the Antennas and Propagation Society Best Paper Award in 1978 and the IEEE Centennial Medal in 1984.